LABORATORY STUDY OF SEA SPRAY FROM BREAKING WAVES:

5.1 PART I - PROFILES OF DROPLET MICROPHYSICAL PROPERTIES

C.W. Fairall[1]*, C.J. Zappa[2], S. Brumer[2], M.L. Banner[3], R.P. Morison[3], X. Yan[4] and W.L Peirson[4].

1. NOAA, Earth System Research Laboratory, Boulder, Colorado, USA; 2. Columbia University, Palisades, NY, USA; 3. University of New South Wales, Sydney, Australia; 4. Water Research Laboratory, University of New South Wales, Manly Vale, Australia

1. INTRODUCTION

In this paper we report on work in the laboratory to develop an accurate sea spray source function parameterization through coincident observations of sea spray along with wave breaking, turbulent kinetic energy dissipation rate, and turbulent fluxes. The laboratory effort is the second rendition of the Spray Production and Dynamics Experiment (SPANDEX) conducted at the Wind Tunnel Facility of the Water Research Laboratory in Manly Vale (NSW, Australia). SPANDEX-I was done in February 2003 and is described in *Fairall et al*. (2009); SPANDEX-II done in June of 2010. SPANDEX-II featured several observational advances compared to SPANDEX-I: direct measurements of ocean-side turbulence profiles and thermal imaging of individual spray drops. Spray drops were measured with an optical array size spectrometer. Properties of the sea spray profiles as a function of forcing will be discussed. We compare these results to a theoretical profile based on a balance of turbulent upward transport and gravitational settling.

2. BACKGROUND ON SPRAY SOURCE

Present parameterizations of air-sea turbulent fluxes are reasonably valid up to wind speeds of about 25 m/s [*Fairall et al.*, 2003; *Drennan et al.*, 2007]. This wind speed range covers the vast majority of oceanic wind climatology.

* *Corresponding author address*: C. W. Fairall, NOAA ESRL R/PSD03, 325 Broadway,Boulder, CO 80305-333, email: Chris.Fairall@noaa.gov

Extrapolations of the current parameterizations to hurricane wind speeds are inconsistent with theoretical analyses of the potential strength of tropical cyclones [*Emanuel*, 1995]. One major issue is the relative balance of momentum and scalar (heat/moisture) transfers – usually expressed as the ratio of the momentum to enthalpy transfer coefficient. It is speculated that the heat and moisture balance is affected by evaporation of sea spray droplets at very high wind speeds (U>25 m/s). At high wind speeds, the ocean is a major source of droplets produced by bursting bubbles and spume (i.e., from sheared-off wave tops) to the lower troposphere [Andreas *et al.*, 1995]. Because of their much larger sizes (and larger mass flux) spume droplets are expected to dominate the hurricane droplet flux problem. Droplets may play a large role in latent heat transfer between the ocean and atmosphere [*Andreas et al.*, 1995] and under extremely high winds such as found in hurricanes, may also have a large effect on the air-sea exchange of momentum [*Andreas and Emanuel*, 2001; *Andreas*, 2004]. From a modeling perspective, there are two fundamental problems: 1) specification of the sea surface droplet source strength and 2) computation (or parameterization) of the thermodynamic effects of the sea spray [*Fairall et al.*, 1990, 1994; *Kepert et al.*, 1999].

The fundamental parameter required for representing the effect of sea spray on air-sea exchange processes is the size dependent *source function,* $S_n(r)$, or number of droplets of a given size produced at the sea surface per unit surface area per unit time, as a function of the surface forcing (wind speed, wave breaking, surface stress, etc) - see *Fairall et al*. (2009) for a

summary. Because the source function cannot be measured directly at present, it is typically estimated from the height-dependent number-size distribution of droplets, $n(r, z)$. The relationship between the source strength, the atmospheric turbulence profiles, the forcing, and the profiles of droplet concentration as a function of droplet size is key to this approach.

3. DROPLET DYNAMICS AND CONCENTRATION PROFILES

3.1 *Turbulent Transport Equations*

In reasonably horizontally homogenous conditions, the aerosol particle conservation equation [*Fairall et al.*, 2009] can be expressed

$$\frac{Dn}{Dt} = -\frac{\partial}{\partial z}\left[\overline{w'n'} - D_p\frac{\partial n}{\partial z} - V_g n + \overline{w_s'n'} + S_n\right] \quad (1)$$

where z is the height above surface, n the size-dependent droplet number concentration, w' the vertical air motion fluctuations, D_p the size dependent droplet molecular diffusion coefficient, V_g the particle mean gravitational settling velocity, w_s' the air-particle slip velocity, and S_n a particle size and height dependent source function (number of particles of a specific size increment created per unit area per second at a specified height). We can then write a conserved flux variable that includes the source terms:

$$F_z = \left[\overline{w'n'} - D_p\frac{\partial n}{\partial z} - V_g n + \overline{w_s'n'} + S_n\right] \quad (2)$$

In steady-state and horizontally homogeneous conditions, the net flux is independent of height.

The production of sea spray droplets is confined very close to the surface in a source region below a height h. Thus, we can deal with the dynamics of interest here by assuming $F_z = F$=constant for heights less than a few times h. Spume droplets are blown off the top of breaking regions near the windward face of the dominant waves; it is clear that h scales with significant wave height [confirmed in SPANDEX-I, *Fairall et al.*, 2009]. For our purposes it is sufficient to consider an area-averaged source of the simplest specification S_n is a constant for $z<h$ and $S_n=0$ for $z>h$.

3.2 *Simple Source and Profile Relationships*

Equation (2) provides a basis to describe the profile of droplets above the source height as a function of drop size:

$$F_z = \overline{w'n'} + \overline{w_s'n'} - V_g n = F = const. \quad (3)$$

Turbulent transport of passive scalars in the surface layer is well-described by a standard eddy-diffusion approach,

$$\overline{w'n'} + \overline{w_s'n'} = -K_p(z)\frac{\partial n}{\partial z} = -\frac{\kappa z u_*}{S_c\phi_c(z/L)}\frac{\partial n}{\partial z} \quad (4)$$

where K_p is the eddy-diffusion coefficient for droplets which combines both the w' and the w_s' covariance terms, u_* is the friction velocity, κ =0.4 is the von Karman constant, S_c is a factor that reduces the diffusion coefficient to account for the inability of large particles to follow turbulent fluctuations exactly, ϕ is the Monin-Obukhov (MO) scalar dimensionless gradient function, and L is the Obukhov length which characterizes the effects of buoyancy on the turbulent diffusivity.

Following Chamecki et al. (2007), (3) and (4) yield a differential equation that relates the particle concentration profile to the flux including the effects of stability

$$\frac{\partial n}{\partial \xi} + \frac{\alpha\phi_c(\xi)}{\xi}[n + F/V_g] = 0 \quad (5)$$

where $\xi = z/L$ and $\alpha = S_c V_g / \kappa u_*$. This can be solved for the flux

$$F = -\frac{\kappa u_*}{S_c}(n_2 - n_h)\frac{\alpha}{1-\exp(-\alpha f)} - V_g n_h \quad (6)$$

and the profile takes the form

$$n_2 = n_h\exp(-\alpha f) + \frac{S_c F}{\kappa u_*}\frac{[\exp(-\alpha f) - 1]}{\alpha} \quad (7)$$

where

$$f = [\ln(z_2/h) - \Psi_c(z_2/L) + \Psi_c(h/L)] \quad (8)$$

For submicron aerosol particles, fall velocity becomes negligible and $\alpha \to 0$ so that (6) reduces to the standard MO equation relating the turbulent flux to the gradient of a scalar. Because of the very strong winds relevant to our wind tunnel study, we have ignored hydrostatic stability effects for the remainder of this paper. For the large droplets of interest here (radius greater than about 10 μm) the turbulent transport tends to be balanced by fall velocity so $F \approx 0$. This gives a simple differential equation with a well-known solution

$$n(z) = n(h)\exp[-\frac{S_c V_g}{\kappa u_*}\ln(z/h)] \quad (9)$$

Thus, we can write

$$S_n = V_g n(h) = V_g n(z)\exp[\frac{S_c V_g}{\kappa u_*}\ln(z/h)] \quad (10)$$

4. SPANDEX DETAILS

4.1 W*ind-Wave Tunnel and Setup*

Observations of spray flux and the underlying breaking waves were made in a wind-wave tank at the Water Research Laboratory. This facility is 30m long, 0.9m wide and 1.55m high [Fig. 1 - see *Fairall et al.* 2009 for details]. Monochromatic waves of small steepness were initiated by an adjustable frequency paddle wave maker, located approximately 3.5m downwind of a large speed controllable fan, which could generate wind speeds typical of strong storms. At its downwind end, the wave tank has a dissipating beach and a duct to discharge the spray outside the laboratory.

The strong wind forcing rapidly amplified the paddle-generated waves, producing a train of heavily breaking waves within a few meters of the paddle. In an effort to maintain a consistency of waveform and energy flux from the wind to the waves, low steepness waves were generated at the paddle. Under the action of the wind, these waves grew in amplitude along the tank but retained their underlying frequency. The fetch where breaking began was set to be similar for each of the wind and wave conditions observed. This was achieved by adjusting the steepness of the initial wave train produced by the paddle. Detailed measurements were undertaken at an observation point located approximately 10m from the paddle. Salt was added to the water to a nominal salinity of 30 psu.

4.2 *Measurements*

4.2.1 *The CIP Droplet Probe*

The SPANDEX study used the Cloud Imaging Probe, CIP manufactured by Droplet Measurement Technologies (DMT) in Boulder, CO, USA. The CIP is a technology based on a linear array of 64 light detecting diodes. As it transits the beam, the particle casts a shadow across the array and the size is deduced from the number of diodes that are occulted. The CIP is set to sample at 1-s time resolution. For the analysis presented in this paper, the counts were totaled for each run and a single spectrum was computed. A smoothing routine was run to simplify the spectrum. Examples of smoothed volume spectra from runs on June 25 for two cases (6.1 cm height and 16.2 cm with weak forcing) are shown in Fig. 2.

For any spectrum we can compute an estimate of the suspended total droplet mass at a given height

$$M(z) = \frac{4\pi\rho_w}{3}\int n(z,r)r^3 dr = \rho_w \int V(r)r^3 dr \quad (11)$$

where ρ_w is the density of seawater water and *V(r)* the volume concentration. Similarly, we can compute an estimate of the gravitation component of the droplet mass flux $F_{gm}(z)$ or an estimate of flux required at the source height, $F_{gm}(h)$, to produce $F_m(z)$

$$F_{gm} = \frac{4\pi\rho_w}{3}\int V_g n(z,r)r^3 dr \quad (12a)$$

$$F_{gm}(h) = \frac{4\pi\rho_w}{3}\int [V_g n(z,r)\exp[\frac{S_c V_g(r)}{\kappa u_*}\ln(z/h)]r^3 dr = S_n \quad (12b)$$

For measurements near wave crests, the mass and mass flux scale as the 3rd and 4th moments of the measured spectrum. As z increases, the weighting factor of larger sizes increases further making estimates of mass and mass flux estimates very sensitive to poor counting statistics.

4.2.2 Other Measurements

Wind speeds in the air cavity were monitored using a hot bulb anemometer mounted from the roof within the air cavity in the upwind section of the tank (Fig. 1). The anemometer was inserted only 0.125 m into the air cavity to minimise any spray influence. The wind stress was determined by measuring the near-surface logarithmic boundary layer profile in the air for each wind speed condition. These were taken at the point of spray measurement within the tank. The velocity profile measurements were made using a small pitot-static (PS) tube. A friction velocity was computed from the wind profile for each forcing condition (Table I). Other nominal conditions in the wind tunnel were monitored: air temperature and relative humidity, water depth, and salinity. A second set of instruments (wave height, fast infrared images, and water-side turbulence) are described elsewhere (Zappa et al. this volume).

4.2.3 Wave conditions and measurements

Two wave paddle frequencies were used during these observations (1.36 Hz and 1.62 Hz), which we are designating as *long* or *short* wavelength. The wave generator initiated a train of narrow bandwidth, low steepness waves, which rapidly amplified under the action of the very strong overlying wind. The waves grew to breaking, with almost every wave breaking actively as it passed the observing station about 10m downwind of the wave paddle. Two wind speeds based on the application of 2 or 3 fans to ventilate the wind tunnel. After some initial testing and general playing around, four sets of forcing conditions were used combining 2 or 3 fans and short or long waves. A summary of the conditions for SPANDEX-II are shown in Fig. 3.

5. RESULTS

5.1 Droplet Concentration Profiles

One goal of SPANDEX-I was to examine the validity of the simplified scaling model of droplet concentration profiles. This was done by measuring concentrations at several heights above mean water for a fixed forcing.

Table 1. Summary of forcing parameters.

Forcing	2Short	2Long	3Short	3Long
u_* (m/s)	0.93	1.02	1.27	1.68
U_{10n} *(m/s)*	20	22	26	31
V_g (m/s)	1.0-2.0	1.7-2.2	1.5-2.0	1.7-2.2
M_0 (g/m^3)	0.06	0.105	0.45	0.85
A	0.92	1.77	1.05	1.63
$\frac{V_g}{\kappa u_*}$	2.7	4.2	3.0	2.5
F_{gm} (g/m^2/s)	0.16	0.23	0.90	1.9

The spectrum at each height, n(z), can be converted to an effective concentration at the source height, n(h), using (9). Sample SPANDEX-I results are shown in Fig. 4. If the assumptions used to derive (9) are valid, then we expect all *corrected* spectra to collapse on a single line. It is clear that evaporation is playing a significant role in deviations from (9) for smaller droplets where there is more spread in the corrected spectra. In Fig. 5 we show a similar example for two spectra from SPANDEX-II. Both the uncorrected and corrected spectra are shown for heights of 16 cm and 25 cm. In this case, it is clear that (9) is over-correcting the higher elevation observations.

Another way to view the profiles is to use the bulk mass or fall velocity flux. Fig. 6 shows profiles for each forcing condition with a power-law fit in the form

$$M = M_0 (z/h)^{-A} \tag{13}$$

If the mass-weighted fall velocity of the spray distribution were independent of height, then we expect $A = S_c V_g / \kappa u_*$. However, because the

concentration of larger drops decreasing faster with height, we expect the mass-weighted fall velocity to also decrease with height. This is confirmed in the observations (not shown) - the range of V_{gm} for each forcing condition is given in Table I. Because the smaller drops that dominate the mass at higher elevations are easier to suspend, we expect A to be smaller than $S_c V_g / \kappa u_*$ (values given in Table I). From forward calculations with the spectra, we expect the mass-slope to be about half the theoretical value.

5.2 *DROPLET SOURCE SCALING*

The dependence of droplet production on the forcing of the system in SPANDEX-I was examined in detail by *Fairall et al*. (2009). Simple scaling in the literature suggest S_n is proportional to wind-speed to some power (3 to 4), whitecap fraction (also, wind-speed to the 3-4 power), friction velocity to some power, or energy lost to wave breaking. This will be discussed in more detail by *Zappa et al.* (this volume), but for our amusement we show estimates of S_n from SPANDEX I and II as a function of u_* in Fig. 7. Note that these results suggest the conditions from SPANDEX-I produce about twice as many drops at the same friction velocity as SPANDEX-II.

6. Conclusions

SPANDEX-I used laboratory data to examine scaling relationships for the vertical profiles and the production of spume sea spray droplets. Those observations of droplet profiles (Fig. 4) give reasonable confirmation of the basic profile relationship (9) that is commonly used to relate droplet concentrations to the surface source strength. The preliminary results from SPANDEX-II do not compare as well. The SPANDEX-II mass profiles do follow a power law in height with the exponent considerably less than the theoretical value appropriate for a fixed drop size (Fig. 6). At the same values of friction velocity the II droplet flux is about half that of I (Fig. 7).

Acknowledgments.

The authors wish to thank the staff of the Water Research Laboratory, School of Civil and Environmental Engineering of the University of New South Wales, for their outstanding efforts that made this study possible. This work was supported by the Office of Naval Research and the NOAA Hurricane Forecast Improvement Program.

References

Andreas, E. L, J.B. Edson, E.C. Monahan, M.P. Rouault, and S.D. Smith (1995), The spray contribution to net evaporation from the sea – A review of recent progress, *Bound.-Layer Meteorol.*, **72**, 3-52.

Andreas, E. L, and K.A. Emanuel (2001), Effects of sea spray on tropical cyclone intensity, *J. Atmos. Sci.*, **58,** 3741-3751.

Andreas EL, Spray stress revisited (2004), *J. Phys. Oceanogr.*, **34**, 1429-1440.

Chamecki, M., R. van Hout, C. Meneveau, and M.B. Parlange, 2007: Concentration profiles of particles settling in the neutral and stratified atmospheric boundary layer. *Bound.-Layer Meteorol.,* **125**, 25-38.

Drennan, W.M., J.A. Zhang, J.R. French, C. McMormick, and P.G. Black (2007), Turbulent fluxes in the hurricane boundary layer. Part II: Latent heat flux. *J. Atmos. Sci.*, **64**, 1103-1115.

Emanuel, K. A. (1995), Sensitivity of tropical cyclones to surface exchange coefficients and a revised steady-state model incorporating eye dynamics. *J. Atmos. Sci.*, **52**, 3969–3976.

Fairall, C.W., J.B. Edson, and M.A. Miller (1990), "Heat fluxes, whitecaps, and sea spray." In *Surface Waves and Fluxes: Current Theory and Remote Sensing*, Eds. G. Geernaert and W. Plant, Reidel Publishing Company, Holland, 173-208.

Fairall, C. W., J. D. Kepert, and G. H. Holland (1994), The effect of sea spray on surface

energy transports over the ocean, *Glob. Atmos. Ocean System*, **2**, 121-142.

Fairall, C. W., E. F. Bradley, J. E. Hare, A. A. Grachev, and J. B. Edson (2003), Bulk parameterization of air-sea fluxes: Updates and verification for the COARE algorithm, *J. Clim.*, **16**, 571-591.

Fairall, C. W., M. Banner, W. Peirson, R. P. Morison, and W. Asher, 2009: Investigation of the physical scaling of sea spray spume droplet production. *J. Geophys., Res*., **114**, C10001, doi:10.1029/2008JC004918.

Kepert, J. D., C. W. Fairall, and J.-W. Bao (1999), Modeling the interaction between the atmospheric boundary layer and evaporating sea spray droplets. *Air-Sea Fluxes: Momentum, Heat, and Mass Exchange*, G. L. Geernaert, Editor, Kluwer, Dordrecht, 363-409.

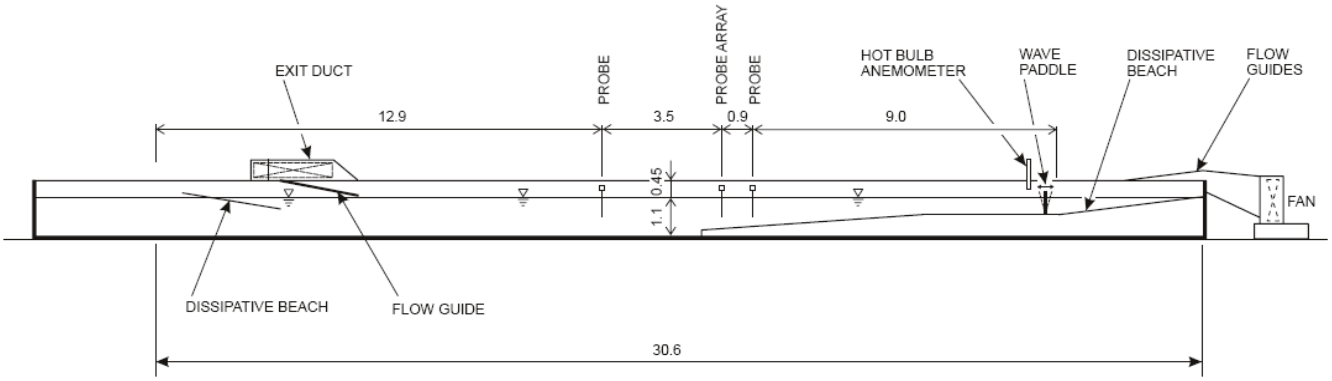

Figure 1. Schematic of wind-wave flume used in this study. All dimensions are in meters.

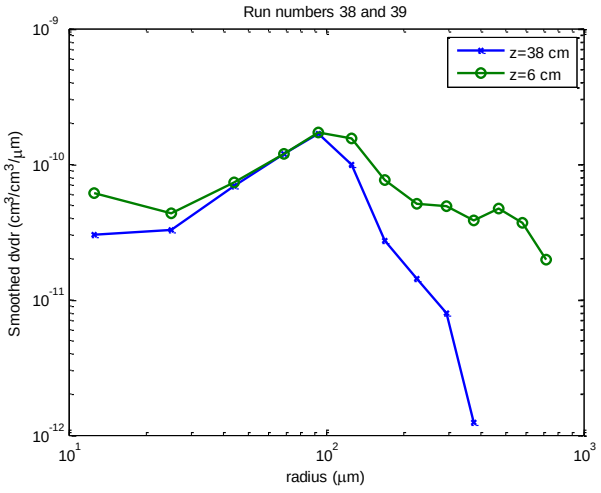

Figure 2. Examples of smoothed volume spectra for two cases (CIP height 6.1 cm and 18.2 cm with weak forcing). The total sample at was 29 minutes long.

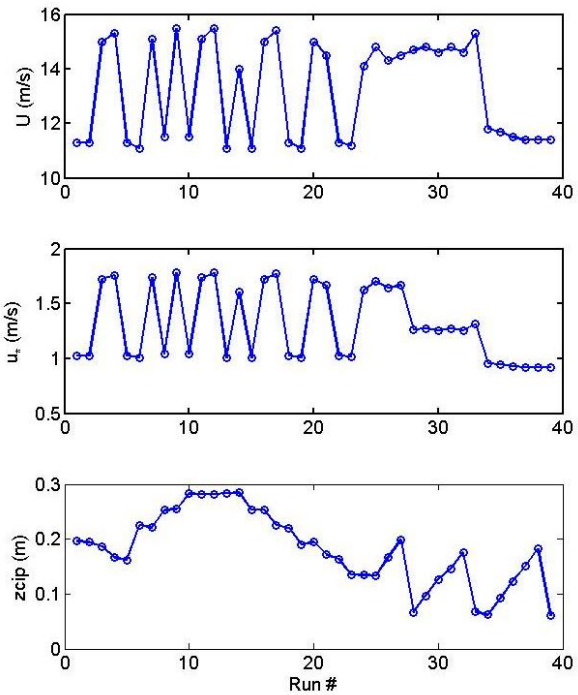

Figure 3. Time series of wind speed, friction velocity, and CIP probe height for SPANDEX-II.

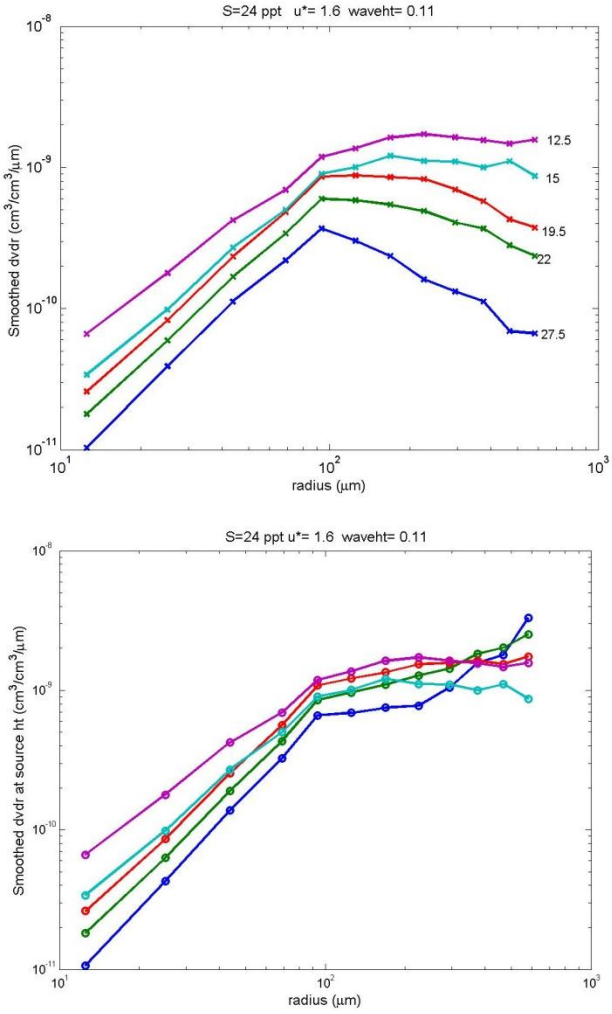

Figure 4. Sample droplet volume size spectra from SPANDEX-I are shown at a nominal forcing condition (u_* ≈1.6 ms^{-1} and h≈ 0.11 m) for water with salinity of 24 ppt. Upper panel – observed spectra where the height of the measurement (cm) above the mean surface is indicated at the side of the curve. Lower panel – spectra corrected to source height via (9).

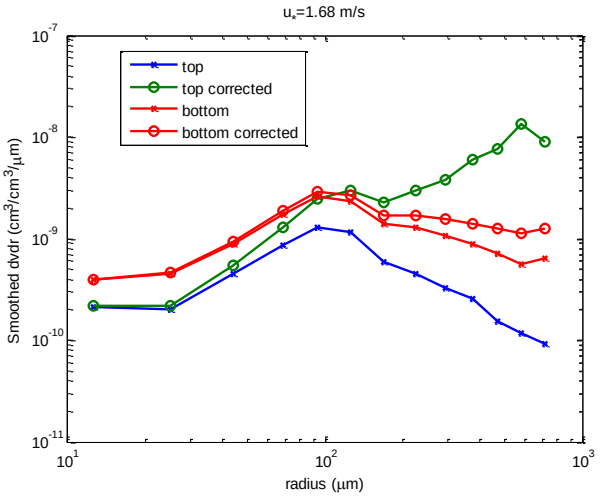

Figure 5. Volume spectra from the top and bottom of the profile for funs 16 (top=25 cm) and 25 (bottom=16 cm). The raw spectra (x's) and corrected to source height (o's) are shown.

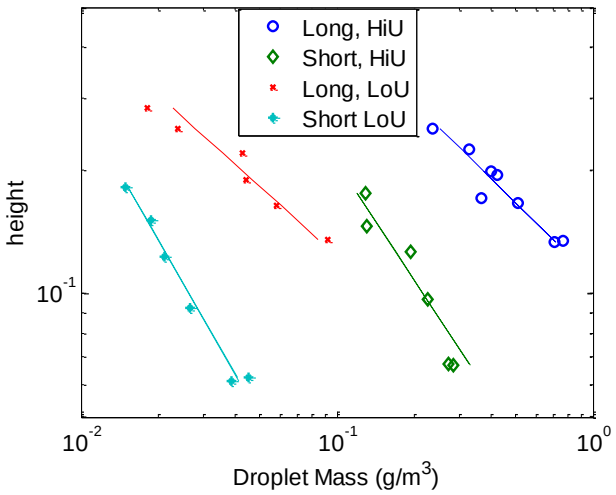

Figure 6. Profiles of droplet mass for four different forcings (see Table I).

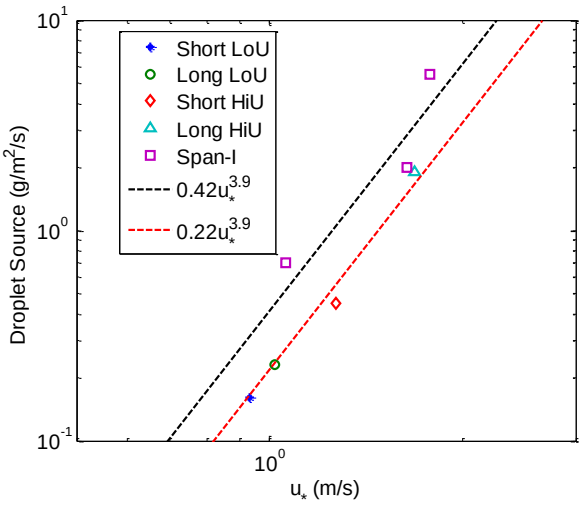

Figure 7. Drop source strength (flux) as a function of u_* for SPANDEX-I and SPANDEX-II.